

LMI-based Mixed H_2/H_∞ Control with Regional Constraints for Spacecraft Attitude Tracking

By Takahiro SASAKI¹⁾⁻³⁾, Takashi SHIMOMURA¹⁾ and Sayaka KANATA¹⁾

¹⁾Department of Aerospace Engineering, Osaka Prefecture University, Osaka, Japan

²⁾Department of Aerospace Engineering Science, University of Colorado Boulder, Colorado, USA

³⁾Research Fellow of Japan Society for the Promotion of Science (DCI)

Satellite dynamics is described by a nonlinear differential equation. Most of recent studies about attitude control have used nonlinear controllers. However, with these controllers, control performance is ignored in most cases. To overcome this problem, this paper applies the linear parameter-varying (LPV) control theory to the attitude control for a spacecraft with reaction wheels (RWs). The LPV control theory can provide a gain-scheduled (GS) controller by using linear matrix inequalities (LMIs) for the mixed $\mathcal{H}_2/\mathcal{H}_\infty$ control which guarantees optimality and robustness at the same time. And also, two types of regional pole placement (RPP) constraints are considered. Through some numerical examples, the effectiveness of these two types of RPP constraints are demonstrated.

Key Words: Attitude Control, RW, LMI, Regional Pole Constraint

Nomenclature

\mathbf{J}	:	inertia matrix of the spacecraft
I_{ws}	:	inertia of wheel spin axis
\mathbf{q}	:	quaternion (Euler Parameters)
$\boldsymbol{\omega}$:	angular velocity vector of the spacecraft
$\boldsymbol{\Omega}$:	wheel spin rate vector
\mathbf{G}_s	:	spin axis matrix
\mathcal{B}	:	body-fixed frame
\mathcal{N}	:	inertial frame
$\boldsymbol{\rho}$:	scheduling parameter vector

Subscripts

0	:	initial
e	:	error
d	:	desired

Superscripts

\times	:	skew-symmetric
----------	---	----------------

1. Introduction

In recent years, attitude control of spacecraft has been studied extensively. They deal with several kinds of actuators such as momentum exchange devices (MEDs) and external torque generators (e. g. gas jets or magnetic torquers). External torque generators have disadvantages such as limited resources or small torque. MEDs have been used for attitude control of spacecraft as actuators, in which they do not require fuel. Since reaction wheels (RWs) can generate control torque precisely, RWs in MEDs are often used for attitude control of spacecraft. Therefore, in this paper, we mainly focus on RWs to realize 3-axis attitude control.

Most of recent studies use Lyapunov function-based controllers to realize attitude control.¹⁾⁻³⁾ With Lyapunov function-based controllers, overall stability of attitude control is always guaranteed, however, control performance is hard to evaluate. To overcome this problem, few studies⁴⁾⁻⁷⁾ attained 3-axis attitude control with Linear Parameter-Varying (LPV) control the-

ory.⁸⁾⁻¹⁰⁾ LPV control theory can provide a gain-scheduled (GS) controller by using linear matrix inequalities (LMIs) for the mixed $\mathcal{H}_2/\mathcal{H}_\infty$ control which guarantees optimality and robustness at the same time. However, this controller design deals with frequency-domain aspects and sometimes provide little transient behavior. By using regional pole placement (RPP) constraint, some research¹¹⁾⁻¹⁵⁾ solves this problem. This paper considers two types of RPP constraints to improve control performance.

The rest of this paper is organized as follows. In Section 2, we show a brief overview of the dynamics and the kinematics of a spacecraft. In Section 3, the generalized LPV model of spacecraft dynamics with RWs shall be established. Section 4 presents two types of RPP constraints to design the GS controller while considering the control performance. In Section 5, some numerical simulation results are given and the effectiveness of two types of RPP constraints are demonstrated. Finally, Section 6 concludes the paper.

2. Spacecraft Model

In this paper, we deal with a spacecraft with RWs as shown in Fig. 1. In this section, a dynamics equation of a spacecraft with RWs is presented. After that, a kinematics equation based on the modified Rodrigues parameters (MRPs) is described.

2.1. Dynamics

The spacecraft considered in this paper is assumed to be a rigid body. Using the definition in Nomenclature, the total angular momentum of a spacecraft with RWs is given as follows:

$$\mathbf{H} = \mathbf{J}\boldsymbol{\omega} + I_{ws}(\mathbf{G}_s\boldsymbol{\Omega}) \quad (1)$$

where

$$\mathbf{G}_s = \begin{bmatrix} 1 & 0 & 0 & -1/\sqrt{3} \\ 0 & 1 & 0 & -1/\sqrt{3} \\ 0 & 0 & 1 & -1/\sqrt{3} \end{bmatrix}. \quad (2)$$

Taking the body-fixed time derivative, the dynamics of a spacecraft is given by

$$\dot{\mathbf{H}} + \omega^\times \mathbf{H} = \mathbf{L}, \quad (3)$$

where the vector \mathbf{L} represents the sum of all the external torques experienced by the spacecraft and the notation ω^\times denotes the following skew-symmetric matrix:

$$\omega^\times := \begin{bmatrix} 0 & -x_3 & x_2 \\ x_3 & 0 & -x_1 \\ -x_2 & x_1 & 0 \end{bmatrix}, \quad \forall \mathbf{x} = [x_1 \ x_2 \ x_3]^T. \quad (4)$$

Substituting Eq. (1) into the first term of Eq. (3), we have

$$\mathbf{J}\dot{\omega} + \mathbf{G}_s I_{ws} \dot{\Omega} + \omega^\times \mathbf{H} = \mathbf{L}. \quad (5)$$

This is the dynamics of a spacecraft with RWs.

2.2. Kinematics

Spacecraft attitude is given by the orientation of the body-fixed frame \mathcal{B} with respect to the inertial frame \mathcal{N} . It is known that three kinematic parameters are enough to describe the attitude. As such parameters, in this paper, the modified Rodrigues parameters (MRPs) are chosen.¹⁶⁾ The MRP vector σ is defined in terms of the Euler parameters as the transformation

$$\sigma_i = \frac{\beta_i}{1 + \beta_0} \quad i = 1, 2, 3. \quad (6)$$

The inverse transformation is given by

$$\beta_0 = \frac{1 - \sigma^T \sigma}{1 + \sigma^T \sigma}, \quad \beta_i = \frac{2\sigma_i}{1 + \sigma^T \sigma}, \quad i = 1, 2, 3. \quad (7)$$

Using the principal rotation axis vector \hat{e} and the rotation angle ϕ , the MRPs are given by

$$\sigma = \tan\left(\frac{\phi}{4}\right) \hat{e}. \quad (8)$$

For such MRPs, the singular points are given at $\theta = \pm 2\pi$. However, these singularities can be avoided to introduce the dual MRP method that consists of the conventional MRP and the shadow MRP.¹⁶⁾ The kinematic equation based on the error MRPs σ_e is given by

$$\dot{\sigma}_e = \mathbf{H}(\sigma_e) \omega_e \quad (9a)$$

$$\mathbf{H}(\sigma_e) = \frac{1}{4} \left[(1 - \sigma_e^T \sigma_e) \mathbf{I}_3 + 2\sigma_e^\times + 2\sigma_e \sigma_e^T \right]. \quad (9b)$$

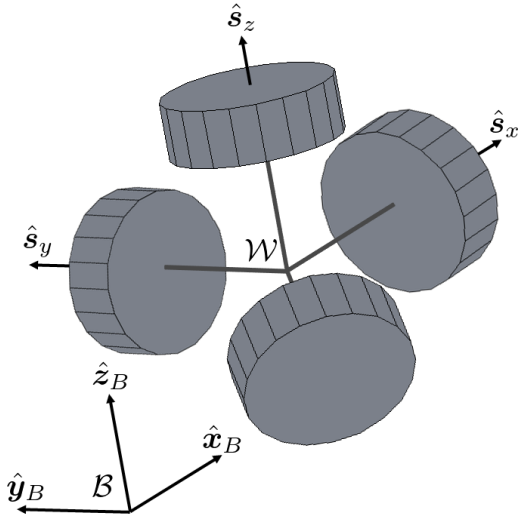


Fig. 1. Tripod configuration of four RWs.

3. LPV Modeling

By introducing the error angular velocity ω_e (see Appendix A) and using Jacobian linearization of Eqs. (5) and (9) around the equilibrium point ($\omega_{e_{eq}} = \mathbf{0}$, $\dot{\Omega}_{e_{eq}} = \mathbf{0}$, $\sigma_{e_{eq}} = \mathbf{0}$), the linearized model of a spacecraft with RWs is described as follows:

$$\begin{bmatrix} \dot{\omega}_e \\ \dot{\sigma}_e \end{bmatrix} = \begin{bmatrix} \mathbf{A}(\rho) & \mathbf{0} \\ \frac{1}{4} \mathbf{I}_3 & \mathbf{0} \end{bmatrix} \begin{bmatrix} \omega_e \\ \sigma_e \end{bmatrix} + \begin{bmatrix} \mathbf{B} \\ \mathbf{0} \end{bmatrix} \mathbf{u} + \begin{bmatrix} \mathbf{E} \\ \mathbf{0} \end{bmatrix} \mathbf{w}, \quad (10)$$

where $\mathbf{E}\mathbf{w}$ is the disturbance term,

$$\mathbf{A}(\rho) = I_{ws} \mathbf{J}^{-1} \rho^\times \quad (11)$$

$$\mathbf{B} = -I_{ws} \mathbf{J}^{-1} \quad (12)$$

$$\mathbf{u} = \mathbf{G}_s \dot{\Omega} \quad (13)$$

with

$$\rho := \mathbf{G}_s \Omega = \begin{bmatrix} \Omega_1 - \frac{1}{\sqrt{3}} \Omega_4 \\ \Omega_2 - \frac{1}{\sqrt{3}} \Omega_4 \\ \Omega_3 - \frac{1}{\sqrt{3}} \Omega_4 \end{bmatrix}. \quad (14)$$

Setting the state variable $\mathbf{x} := [\omega_e^T \ \sigma_e^T]^T$, the state-space representation of Eq. (10) is rewritten as follows:

$$\dot{\mathbf{x}} = \mathbf{A}_e(\rho) \mathbf{x} + \mathbf{B}_e \mathbf{u} + \mathbf{E}_e \mathbf{w}. \quad (15)$$

The Jacobian matrices are defined as

$$\mathbf{A}_e(\rho) := \begin{bmatrix} \mathbf{A}(\rho) & \mathbf{0} \\ \frac{1}{4} \mathbf{I}_3 & \mathbf{0} \end{bmatrix}, \quad \mathbf{B}_e := \begin{bmatrix} \mathbf{B} \\ \mathbf{0} \end{bmatrix}, \quad \mathbf{E}_e := \begin{bmatrix} \mathbf{E} \\ \mathbf{0} \end{bmatrix}. \quad (16)$$

The generalized plant for Eq. (15) is defined as follows:

$$\begin{cases} \dot{\mathbf{x}} = \mathbf{A}_e(\rho) \mathbf{x} + \mathbf{B}_e \mathbf{u} + \mathbf{E}_e \mathbf{w} \\ \mathbf{z} = \mathbf{C} \mathbf{x} + \mathbf{D} \mathbf{u} \end{cases} \quad (17)$$

where the coefficient matrix set (\mathbf{C} , \mathbf{D}) is normally selected that they normally satisfy the condition $\mathbf{C}^T \mathbf{D} = \mathbf{0}$, $\mathbf{D}^T \mathbf{D} > \mathbf{0}$, and where \mathbf{w} and \mathbf{z} are the disturbance input vector and the performance output vector for the simple LPV model in Eq. (15), respectively. This controller is given by

$$\mathbf{u} = -\mathbf{K}(\rho) \mathbf{x}. \quad (18)$$

The LPV system and the GS controller are expressed by the following polytopic representation:

$$\mathbf{A}_e(\rho) = \sum_{i=1}^p \lambda_i(\rho) \mathbf{A}_{ei}, \quad (19)$$

$$\mathbf{K}(\rho) = \sum_{i=1}^p \lambda_i(\rho) \mathbf{K}_i, \quad (20)$$

$$\lambda_i(\rho) \geq 0, \quad \sum_{i=1}^p \lambda_i(\rho) = 1, \quad (21)$$

where p denotes the number of vertices. In this case, p is equal to 8 ($= 2^3$).

4. GS Controller Synthesis

In this section, three types of GS controllers are designed.

4.1. Controller Synthesis without RPP Constraints

Let us introduce the following mixed $\mathcal{H}_2/\mathcal{H}_\infty$ LMI problem:⁸⁾

$$\inf_{W_i, X, Z} [\text{Trace}(\mathbf{Z})] \quad \text{subject to} \quad (22a)$$

$$\Psi_{H2} > 0, \quad \Psi'_{H2} < 0, \quad (22b)$$

$$\Psi_{H\infty} < 0, \quad (22c)$$

for all $1 \leq i \leq p$,

where

$$\Psi_{H2} = \begin{bmatrix} X & * \\ E_e^T & Z \end{bmatrix},$$

$$\Psi'_{H2} = \begin{bmatrix} (A_{ei}X - B_e W_i) + (\bullet)^T & * \\ CX - DW_i & -I \end{bmatrix},$$

$$\Psi_{H\infty} = \begin{bmatrix} (A_{ei}X - E_e W_i) + (\bullet)^T & X C^T - W_i D^T & E_e \\ * & -\gamma I & D \\ * & * & -\gamma I \end{bmatrix},$$

Eqs. (22a) and (22b) guarantee the \mathcal{H}_2 performance and Eq. (22c) gives the \mathcal{H}_∞ constraint. Using the optimal solution sets X , W_i to the problem of Eqs. (22), the extreme controllers K_i at each vertex of the operation range are given by

$$K_i = W_i X^{-1}, \quad 1 \leq i \leq p. \quad (23)$$

Then, the GS controller is constructed by substituting Eq. (23) into Eq. (20).

Note that the common Lyapunov solution $X > 0$ was used in the past GS controller design and resulted in conservatism. As an alternative, we use another method,¹⁰⁾ in which the distinct Lyapunov solutions $X_i > 0$ are adopted. Then, we have

$$\inf_{W_i, X_i, Z_i} [\text{Trace}(\mathbf{Z}_i)] \quad \text{subject to} \quad (24a)$$

$$\tilde{\Psi}_{H2} > 0, \quad \tilde{\Psi}'_{H2} < 0, \quad (24b)$$

$$\tilde{\Psi}_{H\infty} < 0, \quad (24c)$$

for each $1 \leq i \leq p$,

where

$$\tilde{\Psi}_{H2} = \begin{bmatrix} X_i & * \\ E_e^T & Z_i \end{bmatrix}$$

$$\tilde{\Psi}'_{H2} = \begin{bmatrix} (A_{ei}X_i - B_e W_i) + (\bullet)^T & * \\ C X_i - D W_i & -I \end{bmatrix}$$

$$\tilde{\Psi}_{H\infty} = \begin{bmatrix} (A_{ei}X_i - E_e W_i) + (\bullet)^T & X_i C^T - W_i D^T & E_e \\ * & -\gamma I & D \\ * & * & -\gamma I \end{bmatrix}.$$

Using the optimal solution sets (X_i, W_i) to the problem of Eqs. (24), less conservative extreme controllers can be obtained. The extreme controllers are given by

$$K_i = W_i X_i^{-1}, \quad 1 \leq i \leq p. \quad (25)$$

By using these extreme controllers, a GS controller is again constructed as in Eq. (20). In order to guarantee overall stability and control performance in a whole operation range, we seek a

common Lyapunov solution $X_c > 0$ that satisfies the following LMIs:

$$\inf_{X_c, Z} [\text{Trace}(\mathbf{Z})] \quad \text{subject to} \quad (26a)$$

$$\tilde{\Psi}_{H2} > 0, \quad \tilde{\Psi}'_{H2} < 0, \quad (26b)$$

$$\tilde{\Psi}_{H\infty} < 0, \quad (26c)$$

for all $1 \leq i \leq p$,

where

$$\tilde{\Psi}_{H2} = \begin{bmatrix} X_c & * \\ E^T & Z \end{bmatrix},$$

$$\tilde{\Psi}'_{H2} = \begin{bmatrix} (A_{ei} - B_e K_i)X_c + (\bullet)^T & * \\ (C - D K_i)X_c & -I \end{bmatrix},$$

$$\tilde{\Psi}_{H\infty} = \begin{bmatrix} (A_{ei} - E_e K_i)X_c + (\bullet)^T & X_i C^T - K_i X_c D^T & E_e \\ * & -\gamma I & D \\ * & * & -\gamma I \end{bmatrix}.$$

4.2. Controller synthesis with RPP Constraints # 1

Region # 1^{11), 15)} is the set $S(\alpha, r, \Theta)$ of complex numbers $x + jy$ such that

$$x < -\alpha < 0, \quad |x + jy| < r, \quad \tan \Theta x < -|y| \quad (27)$$

as shown in Fig. 2. Confining the closed-loop poles to this region ensure a minimum decay rate α , a minimum damping ratio $\zeta = \cos \Theta$, an undamped natural frequency $\omega_d < r \sin \theta$ and a damped natural frequency $\omega_n < r$. This in turn bounds the maximum overshoot, the frequency of oscillatory modes, the delay time, the rise time, and the settling time. LMIs for the mixed $\mathcal{H}_2/\mathcal{H}_\infty$ control with RPP Constraints #1 are given by

$$\inf_{W_i, X_i, Z_i} [\text{Trace}(\mathbf{Z}_i)] \quad \text{subject to} \quad (28a)$$

$$\tilde{\Psi}_{H2} > 0, \quad \tilde{\Psi}'_{H2} < 0, \quad (28b)$$

$$\tilde{\Psi}_{H\infty} < 0, \quad (28c)$$

$$(A_{ei}X_i - B_e W_i) + (\bullet)^T + 2\alpha X_i < 0, \quad (28d)$$

$$\begin{bmatrix} -rX_i & A_{ei}X_i - B_e W_i \\ * & -rX_i \end{bmatrix} < 0, \quad (28e)$$

$$\begin{bmatrix} \Phi_i(\Theta) & \Phi'_i(\Theta) \\ * & \Phi_i(\Theta) \end{bmatrix} < 0, \quad (28f)$$

for each $1 \leq i \leq p$,

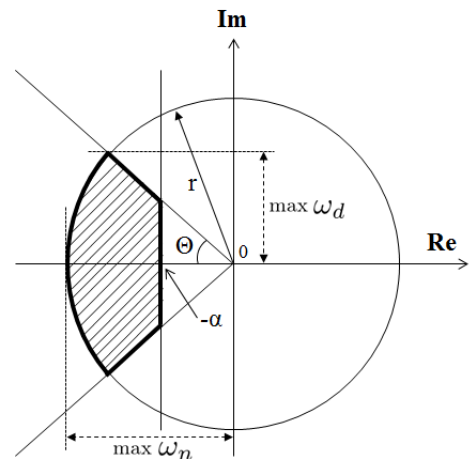


Fig. 2. Regional pole placement #1.

where

$$\Phi_i(\Theta) = \sin \Theta \left\{ (A_{ei}X_i - B_e W_i) + (\bullet)^T \right\} \quad (29)$$

$$\Phi'_i(\Theta) = \cos \Theta \left\{ (A_{ei}X_i - B_e W_i) - (\bullet)^T \right\}. \quad (30)$$

Eqs. (28d)-(28f) are described as RPP Constraints #1. In order to guarantee overall stability and control performance in a whole operation range, we seek a common Lyapunov solution $X_c > 0$ that satisfies the following LMIs:

$$\inf_{X_c, Z} [\text{Trace}(Z)] \quad \text{subject to} \quad (31a)$$

$$\bar{\Psi}_{H2} > 0, \quad \bar{\Psi}'_{H2} < 0, \quad (31b)$$

$$\bar{\Psi}_{H\infty} < 0, \quad (31c)$$

$$(A_{ei} - B_e K_i)X_c + (\bullet)^T + 2\alpha X_c < 0, \quad (31d)$$

$$\begin{bmatrix} -rX & (A_{ei} - B_e K_i)X_c \\ * & -rX_c \end{bmatrix} < 0, \quad (31e)$$

$$\begin{bmatrix} \bar{\Phi}_i(\Theta) & \bar{\Phi}'_i(\Theta) \\ * & \bar{\Phi}_i(\Theta) \end{bmatrix} < 0, \quad (31f)$$

for all $1 \leq i \leq p$,

where

$$\bar{\Phi}_i(\Theta) = \sin \Theta \left\{ (A_{ei} - B_e K_i)X_c + (\bullet)^T \right\} \quad (32)$$

$$\bar{\Phi}'_i(\Theta) = \cos \Theta \left\{ (A_{ei} - B_e K_i)X_c - (\bullet)^T \right\}. \quad (33)$$

4.3. Controller synthesis with RPP Constraints # 2

Region # 2¹⁴⁾ consider circle LMI region D :

$$D_{q,r} = \{x + jy \in C : (x + q)^2 + y^2 < r'^2\} \quad (34)$$

centered at $(-q, 0)$ and with radius $r' > 0$, where the characteristic function is given by

$$f_D(z) = \begin{bmatrix} -r' & z + q \\ \bar{z} + q & -r' \end{bmatrix} \quad (35)$$

As shown in Fig. 3, if $\lambda = -\zeta\omega_n + j\omega_d$ is a complex pole lying in $D_{q,r}$ with damped ratio ζ , undamped natural frequency ω_n , damped natural frequency ω_d , then $\zeta = \sqrt{1 - \left(\frac{r'}{r'+q}\right)^2}$, $\omega_n < q + r$, and $\omega_d < r$. Therefore, this circle region puts a lower bound on both exponential decay rate and the damping ratio of the closed-loop response, and this is very common in practical control design.

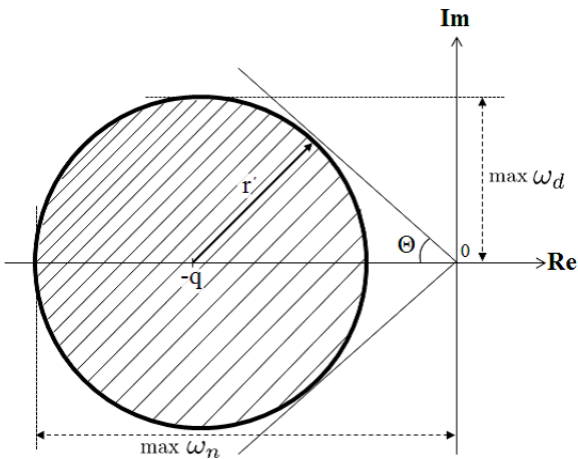


Fig. 3. Regional pole placement #2.

$$\inf_{W_i, X_i, Z_i} [\text{Trace}(Z_i)] \quad \text{subject to} \quad (36a)$$

$$\tilde{\Psi}_{H2} > 0, \quad \tilde{\Psi}'_{H2} < 0, \quad (36b)$$

$$\tilde{\Psi}_{H\infty} < 0, \quad (36c)$$

$$\begin{bmatrix} -r'X_i & qX_i + (A_{ei}X_i - B_e W_i) \\ * & -r'X_i \end{bmatrix} < 0 \quad (36d)$$

for each $1 \leq i \leq p$.

In order to guarantee overall stability and control performance in a whole operation range, we seek a common Lyapunov solution $X_c > 0$ that satisfies the following LMIs:

$$\inf_{X_c, Z} [\text{Trace}(Z)] \quad \text{subject to} \quad (37a)$$

$$\bar{\Psi}_{H2} > 0, \quad \bar{\Psi}'_{H2} < 0, \quad (37b)$$

$$\bar{\Psi}_{H\infty} < 0, \quad (37c)$$

$$\begin{bmatrix} -r'X_c & qX_c + (A_{ei} - B_e K_i)X_c \\ * & -r'X_c \end{bmatrix} < 0, \quad (37d)$$

for all $1 \leq i \leq p$,

Note that from Fig. 3, it has the following constraint:

$$r' = q \sin \Theta. \quad (38)$$

5. Numerical Simulation

This section presents some numerical simulations of the attitude tracking problem given by the satellite in a near-polar orbit found in References.^{17), 18)} The pointing axis is required to track a ground station and the spacecraft is required to rotate about this pointing vector so that the solar panel axis is perpendicular to the spacecraft-sun axis. We present numerical simulations with three types of GS controllers including in GS controller without RPP constraints, with RPP constraints #1, and with RPP constraints #2.

The simulation parameters, the initial conditions (three cases) are given in Table 1. The controller design parameters C , D and the disturbance coefficient matrix E_e are given by

$$C = \begin{bmatrix} 5 \times I_3 & 0_{3 \times 3} \\ 0_{3 \times 3} & I_3 \\ 0_{4 \times 3} & 0_{4 \times 3} \end{bmatrix}, \quad D = \begin{bmatrix} 0_{6 \times 4} \\ 0.02 \times I_4 \end{bmatrix},$$

$$E_e = \begin{bmatrix} 10^{-6} \times \text{diag}[6 \ 9 \ 6] \\ 0_{3 \times 3} \end{bmatrix}. \quad (39)$$

Note that the disturbance coefficient matrix is determined by maximum value of the disturbance torque. The orbital elements or the disturbance torque are written in Appendix B.

Table 1. Simulation parameters.

Symbol	Value	Unit
J	$\text{diag}[10 \ 10 \ 8]$	$[\text{kgm}^2]$
I_{ws}	0.002	$[\text{kgm}^2]$
$\omega_e(0)$ (Case 1)	$[0.02 \ -0.01 \ 0.02]^T$	$[\text{rad/s}]$
$\sigma_e(0)$ (Case 1)	$[0.2 \ -0.2 \ -0.6]^T$	–
$\omega_e(0)$ (Case 2)	$[-0.05 \ 0.04 \ -0.1]^T$	$[\text{rad/s}]$
$\sigma_e(0)$ (Case 2)	$[0.3 \ -0.3 \ 0.6]^T$	–
$\omega_e(0)$ (Case 3)	$[-0.03 \ -0.03 \ -0.03]^T$	$[\text{rad/s}]$
$\sigma_e(0)$ (Case 3)	$[-0.4 \ 0.3 \ -0.4]^T$	–

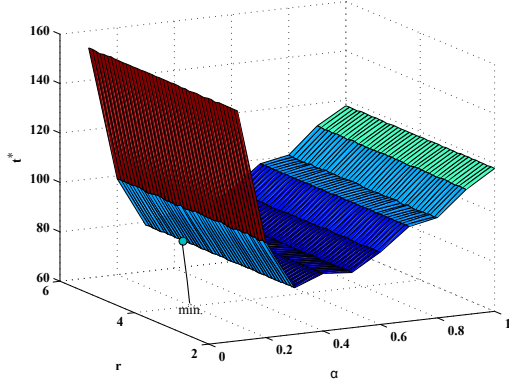


Fig. 4. Parameters of RPP #1 (Case 1).

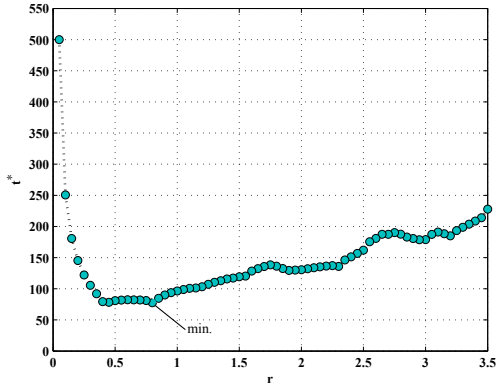


Fig. 5. Parameter of RPP #2 (Case 1).

The steering law in this paper is given as follows:

$$\dot{\Omega} = G_s^T (G_s G_s^T)^{-1} u. \quad (40)$$

It is known that preferred damping ratio range is given by $0.6 < \zeta < 0.8$. In this paper, Θ in RPP #1 and RPP #2 is given by 45 deg (in this case, $\zeta = 0.73$). Using this parameter Θ , unknown parameters are represented by only α, r in RPP #1 and r' in RPP #2. This paper decides these unknown parameters α, r, r' by simulation results in Case 1. Figures 4 and 5 show the relationship between the unknown parameters and convergence time of attaining 3-axis attitude control. From these figures, the minimum time convergence points is given and the parameters α, r, r' are decided as

$$\alpha = 0.3, \quad r = 5, \quad r' = 0.8.$$

The simulation result in Case 1 by using the GS controller without RPP constraints are shown in Fig. 6. The simulation results in Case 1 by using the GS controller with RPP #1 and RPP #2 are shown in Figs. 7 and 8, respectively. Figure 9 shows pole placement results of these controllers in Case 1. And Table 2 shows the convergence time of simulation results. From these figures and table, the convergence time by using the GS controller with RPP are shorter than that by using the GS controller without RPP. Then, the effectiveness of the GS controller with RPP is demonstrated. Regarding RPP #1 and RPP #2, these control performance are almost the same from Figs. 7, 8 and Table 2. From the practical point of view, RPP #2 is easily to decide the parameter and it is easy-to-use constraints.

Table 2. Convergence time [s].

-	$\mathcal{H}_2/\mathcal{H}_\infty$	RPP #1	RPP #2
Case 1	308.05	78.58	78.27
Case 2	278.94	93.08	94.01
Case 3	324.47	85.60	89.54

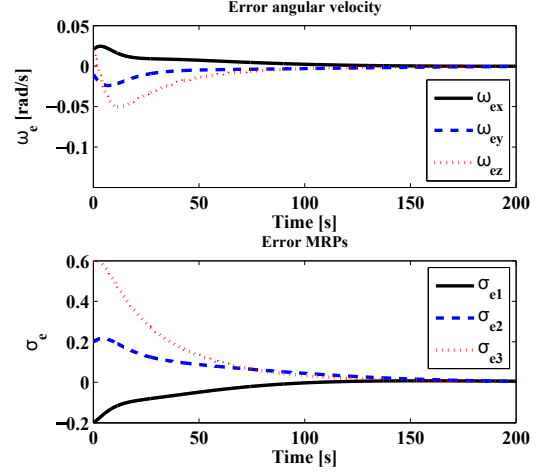


Fig. 6. Attitude control without RPP (Case 1).

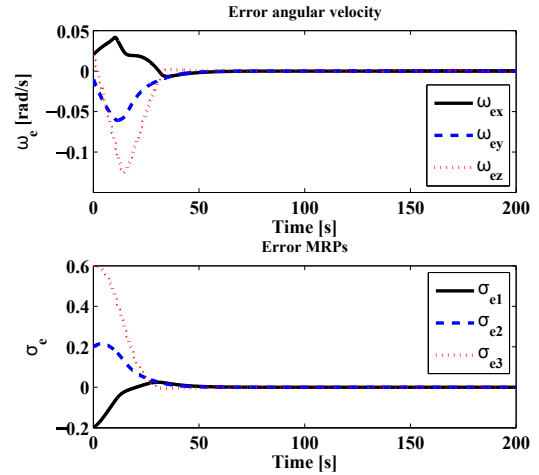


Fig. 7. Attitude control with RPP #1 (Case 1).

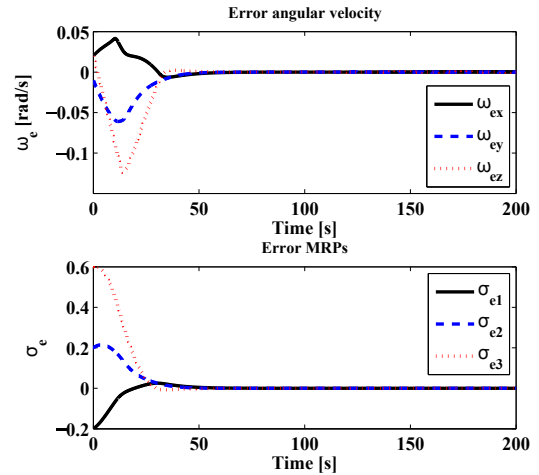


Fig. 8. Attitude control with RPP #2 (Case 1).

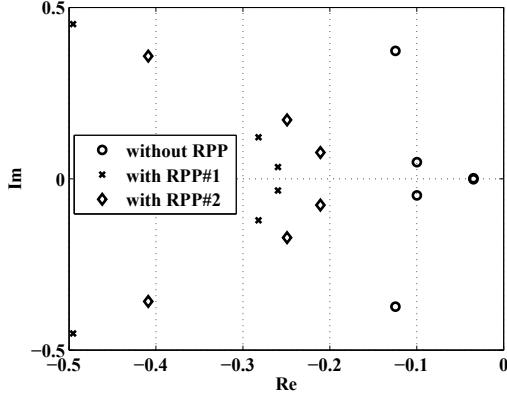


Fig. 9. Pole placement (Case 1).

6. Conclusion

In this paper, an LPV model for 3-axis attitude control of a spacecraft with RWs has been established. Based on this LPV model, three types of GS controllers have been developed by using LMIs for the mixed $\mathcal{H}_2/\mathcal{H}_\infty$ control with/without regional pole placement constraints. Through some numerical examples, the efficiency of the regional pole placement constraints is demonstrated. As a result, an easy-to-use regional pole placement constraint is proposed.

Acknowledgments

This work was supported by JSPS Grant-in-Aid for Scientific Research Grant Numbers 15J11371 and (C)15K06149.

References

- 1) Tsiotras, P.: Stabilization and Optimality Results for the Attitude Control Problem, *Journal of Guidance, Control, and Dynamics*, **19** (1996), pp. 772-779.
- 2) Yoon, H., Tsiotras, P.: Spacecraft Line-of-Sight Control Using a Single Variable-Speed Control Moment Gyro, *Journal of Guidance, Control, and Dynamics*, **29** (2006), pp. 1295-1308.
- 3) Schaub, H., Lappas, V., J.: Redundant Reaction Wheel Torque Distribution Yielding Instantaneous L_2 Power-Optimal Attitude Control, *Journal of Guidance, Control, and Dynamics*, **32** (2009), pp. 1269-1276.
- 4) Kwon, S., Shimomura, T., Okubo, H.: Pointing control of spacecraft using two SGCMGs via LPV modeling theory, *Acta Astronautica*, **68** (2011), pp. 1168-1175.
- 5) Sasaki, T., Shimomura, T.: Attitude Control of A Spacecraft with A Double-Gimbal Variable-Speed Control Moment Gyro via LPV Control Theory, *Advances in the Astronautical Sciences*, **153** (2015), pp. 707-723.
- 6) Sasaki, T., Shimomura, T., Kanata, S.: Spacecraft Attitude Control with RWs via LPV Control Theory: Comparison of Two Different Methods in One Framework, *Transactions of The Japan Society for Aeronautical and Space Sciences, Aerospace Technology Japan*, **14** (2016), pp. 15-20.
- 7) Sasaki, T., Shimomura, T.: Gain-Scheduled Control/Steering Design for a Spacecraft with Variable-Speed Control Moment Gyros, *Journal of Control, Measurement, and System Integration*, **10** (2017), pp. 1-6.
- 8) Khargonekar, P., P., Rotea, M., A.: Mixed $\mathcal{H}_2/\mathcal{H}_\infty$ Control: A Convex Optimization Approach, *IEEE Transactions on Automatic Control*, **36** (1991), pp. 824-837.
- 9) Apkarian, P., Gahinet, P., Becker, G.: Self-Scheduled \mathcal{H}_∞ Control of

Linear Parameter-Varying Systems: A Design Example, *Automatica*, **31** (1995), pp. 1251-1261.

- 10) Shimomura, T., Kubotani, T.: Gain-Scheduled Control under Common Lyapunov Functions: Conservatism Revisited, *Proceedings of 2005 American Control Conference*, 2005, pp. 870-875.
- 11) Chilali, M., Gahinet, P.: \mathcal{H}_∞ Design with Pole Placement Constraints: An LMI Approach, *IEEE Transactions on Automatic Control*, **41** (1996), pp. 358-367.
- 12) Chilali, M., Gahinet, P., Apkarian, P.: Robust Pole Placement in LMI Regions, *IEEE Transactions on Automatic Control*, **44** (1999), pp. 2257-2270.
- 13) Rao, P., S., Sen, I.: Robust Pole Placement Stabilizer Design using Linear Matrix Inequalities, *IEEE Transactions on Power Systems*, **15** (2000), pp. 313-319.
- 14) Hong, S., K., Nam, Y.: Stable Fuzzy Control System Design with Pole-Placement Constraint: An LMI Approach, *Computers in Industry*, **51** (2003), pp. 1-11.
- 15) Shimomura, T., Fujii, T.: Multiobjective Control Design via Successive Over-Bounding of Quadratic Terms, *Int. J. Robust Nonlin. Contr.*, **15** (2005), pp. 363-381.
- 16) Schaub, H., Junkins, J., L.: Stereographic Orientation Parameters for Attitude Dynamics: A Generalization of the Rodrigues Parameters, *Journal of the Astronautical Sciences*, **44** (1996), pp. 1-19.
- 17) Tsiotras, P., Shen, H., Hall, C.: Satellite Attitude Control and Power Tracking with Energy/Momentum Wheels, *Journal of Guidance, Control, and Dynamics*, **24** (2001), pp. 23-34.
- 18) Yoon, H., Tsiotras, P.: Spacecraft Adaptive Attitude and Power Tracking with Variable Speed Control Moment Gyroscopes, *Journal of Guidance, Control, and Dynamics*, **25** (2002), pp. 1081-1090.
- 19) Sidi, M.: Spacecraft Dynamics and Control, A Practical Engineering Approach, Cambridge Univ. Press, New York, (1997).

Appendix A: Error angular velocity

To introduce the reference angular velocity vector $\omega_{\mathcal{R}/\mathcal{N}}$ of the reference frame \mathcal{R} relative to \mathcal{N} , the error angular velocity ω_e is defined by

$$\omega_e = \omega - [\mathcal{BR}]\omega_{\mathcal{R}/\mathcal{N}}. \quad (41)$$

The body-fixed frame time derivative of ω_e are given by

$$\dot{\omega}_e = \dot{\omega} - ([\mathcal{BR}]\dot{\omega}_{\mathcal{R}/\mathcal{N}} - \omega^\times[\mathcal{BR}]\omega_{\mathcal{R}/\mathcal{N}}). \quad (42)$$

Appendix B: Orbital element and disturbance torque

Keplerian elements are shown in Table 3.^{17), 18)} Note that $n, M_0, \omega', \Omega', i, e$ are mean motion, mean anomaly, argument of perigee, right ascension of the ascending node, inclination and eccentricity, respectively. The disturbance torque¹⁹⁾ experienced by aerodynamics, solar pressure, magnetic torque, and other environmental factors is assumed by

$$\mathbf{L} = \begin{bmatrix} 4 \times 10^{-6} + 2 \times 10^{-6} \sin(nt) \\ 6 \times 10^{-6} + 3 \times 10^{-6} \sin(nt) \\ 3 \times 10^{-6} + 3 \times 10^{-6} \sin(nt) \end{bmatrix}. \quad (43)$$

Table 3. Orbital elements.

Symbol	Value	Unit
n	14.57788549	[rev/day]
M_0	234.7460	[deg]
ω'	125.5766	[deg]
Ω'	132.8782	[deg]
i	86.5318	[deg]
e	0.00216220	-